



Theoretical tool for evaluating induction periods of calcium sulfate scaling on reverse osmosis membranes

Abraham Sagiv^a, Xianhui Li^b, Raphael Semiat^a, Hilla Shemer^{a,*}

^aRabin Desalination Laboratory, Wolfson Faculty of Chemical Engineering, Technion-Israel Institute of Technology, Haifa 32000, Israel, Tel. +972 4 8292488; email: shilla@technion.ac.il (H. Shemer), sagiv.ar@gmail.com (A. Sagiv), cesemiat@technion.ac.il (R. Semiat)

^bKey Laboratory for City Cluster Environmental Safety and Green Development of the Ministry of Education, School of Ecology, Environment and Resources, Guangdong University of Technology, Guangzhou 510006, P.R. China, email: lixianhui@gdut.edu.cn

Received 2 February 2022; Accepted 17 March 2022

ABSTRACT

The objective of the study was to provide an evaluation tool for the induction period of reverse osmosis membrane scaling by calcium sulfate. The proposed tool may be used as a preventive measure against severe and irreversible membrane scaling. Scaling experiments were conducted at different Reynolds numbers (Re) and calcium sulfate concentrations, that is, various saturation indices (SI). The observed induction periods were determined at the onset of the permeate flux decline. A computational fluid dynamics model was developed to determine the induction period based on two adjustable parameters describing the balance between deposition and removal rates to and from the membrane surface. These parameters were derived by fitting the model to the experimental results. For a given membrane permeability, solution SI and Re number, a theoretical permeate flux and induction period were calculated using the model. In addition, the model output included the membrane surface coverage by the calcium sulfate scale. Finally, evaluated induction periods (EIP) were determined, considering the average standard deviation between the observed and theoretical induction periods. The average surface coverage fraction of scaling during the induction periods was found to be 0.066 ± 0.034 . The EIP decreases with the supersaturation of the solution and increases with the Re number. EIP values were found to be less than the observed induction periods, satisfying safe operating conditions from both economic and membrane integrity aspects.

Keywords: Desalination; Membrane fouling; Scale deposition; Flux decline; Crystallization

1. Introduction

Scaling of membranes is a major problem that hinders desalination of seawater, brackish water, and wastewater, yielding substantial economic losses. In desalination plants, scaling is usually observed initially at the tail of the reverse osmosis membrane element [1]. This is due to an increased concentration of sparingly soluble salts (such as calcium

carbonate, calcium sulfate, silica, etc.) along the last membrane in a series, leading to supersaturation conditions [2].

It is well established that membrane scaling occurs through both deposition of crystals, formed in the bulk solution, onto the membrane surface (bulk deposition) and surface crystallization (i.e., heterogeneous nucleation on the membrane surface followed by crystal growth). The scaling mechanisms of reverse osmosis (RO) membranes are extensively reviewed elsewhere [3–7].

* Corresponding author.

The permeate flux, as well as membrane strength and endurance, are affected by scaling. Models were developed to describe the scaling process and correlate it to the permeate flux decline. Ruiz-García et al. [8] reviewed predictive models for estimating the permeate flux decline over time due to long-term variation in the water permeability coefficient of the membranes, as a result of compaction and fouling. The models reviewed are based on extended experience of desalination plants operations. Correlation of flux decline data to membrane surface blockage [9–11], mass of salt deposited on the membrane [12], and density and thickness of the deposit [13] are more fundamental models. Others used crystallization theory to model the effects of scale formation on the RO process [14–17].

Determination of the onset of scaling is an important design and control tool. It can be used to:

- Determine the upper limit of the water recovery. High water recovery enables energy, economic, and environmental benefits.
- Help regulate periodic cleaning as a preventive measure against severe and irreversible membrane scaling. In practice, a cleaning sequence is initiated if the normalized permeate flow drops by $\geq 10\%$; the normalized salt rejection decreases by $\geq 10\%$; and/or the normalized differential pressure increases by $\geq 15\%$ [18].
- Design an efficient scale inhibition treatment program. Obviously, avoidance of scaling is desirable as it may not only cause the phenomena mentioned above, but it may also physically damage the membrane as crystal may have very sharp edges.

The term “crystallization induction period” is used to describe the time elapsed between the establishment of supersaturation and the first observed changes in the system’s physical properties due to the formation of a solid phase [19]. The first appearance of a new solid phase, ideally nuclei with the critical cluster size, is related to the detectable limit of the applied size measurement technique [20]. In practice, scaling is preceded by an induction period during which no significant changes in the system operation parameters are observed [2]. In the study described herein, the induction period is defined as the time elapsed between the initiation of desalination and the first observed change in the permeate flux. It is assumed that the processes governing the induction period, at which no significant flux decline is observed, include transport of particles to the membrane surface, net attachment of particles at the surface, removal of part of already deposited material from the membrane surface, and surface crystallization [21].

The presence of very small particles/nuclei, detected by scanning electron microscopy, in bulk solution and on the surface of polyamide RO membrane, was interpreted as evidence of a lack of induction period [22,23]. Nevertheless, none of the commonly monitored parameters (including turbidity, permeate flux, and pH) indicate scaling. It was further concluded that the total deposit mass flux was not affected by the small particles carried by the feed stream. Though, the mechanism of surface crystallization and bulk deposition was confirmed by the experimental data

presented by the authors. In practice, detection of micron-sized crystals in an entire multi-vessel desalination plant and, in particular, in an individual membrane element is extremely difficult. It should further be noted that uneven absolute flux is a characteristic of pressure vessels, and therefore some tail-end membrane elements in a certain pressure vessel are more prone to scaling than others [1]. This means that while scaling may be initiated on some membranes, others may still be unaffected.

Scale formation is being mitigated by applying scale-inhibitors, cleaning, and pH control. These measures may extend the induction period, but not eliminate it. Recent studies investigated parameters affecting the induction period other than the addition of scale-inhibitors, including the saturation indices, Reynolds number, and initial membrane permeability. Experiments revealed that the induction periods increase with augmentation Re number and decrease with increasing saturation indices [2]. A model that identifies scaling-free operating conditions (i.e., induction period) by analyzing the time required for salt molecules to pass through an RO module with the nucleation induction times of the potential scalants was developed by Turek et al. [24]. Simulation revealed longer induction periods as the concentration of calcium sulfate at the exit end of the module increased.

The objective of this research was to develop a numerical computational fluid dynamics (CFD) model as a theoretical tool for evaluating the induction periods of scaling on RO membranes. Two model parameters, reflecting the scale removal and deposition rates, were derived by fitting the theoretical water flux to experimental data, after which the induction period was determined for varying flow conditions and calcium sulfate concentrations. The average standard deviation between the observed and theoretical induction periods was used to calculate an evaluated induction period. A calcium sulfate scale was chosen as a model compound. The net deposition component of the present CFD model is based on the approach of Kern and Seaton [25] in which the overall mass deposited along the membrane surface, at a certain time, is the difference between the mass deposition rate on the membrane surface and the mass removal rate from the surface. Other parts of the CFD model include analysis of the solution flow and its solute convection and diffusion within the bulk that determine the required conditions for the solute deposition dynamics on the membrane surface.

2. Experimental

Experiments were conducted at different saturation indices of CaSO_4 ranging from 1.8 to 4.2 (corresponding to 0.035–0.060 mol/L of CaSO_4) and Reynolds numbers from 404 to 6902 (corresponding to flow rates of 0.4–7.0 L/min). The membrane permeability ranged for, $4\text{--}12 \times 10^{-12}$ m/s Pa. The permeate flux was measured as a function of time. The indication of the onset of scaling was determined by the permeate flux decline due to scale partial coverage of the membrane surface. The experimental system (Tubular module MIC 240), equipped with a polyamide AFC99 RO membrane (CPI membranes, UK) is described in detail elsewhere [2]. The solution was prepared by

dissolving analytical grade $\text{CaCl}_2 \cdot 2\text{H}_2\text{O}$ (Spectrum chemical, USA) and Na_2SO_4 (Bio-Lan Ltd., Israel) in de-ionized water.

The saturation index and Re number were calculated as follows:

$$\text{SI} = \frac{\{\text{Ca}^{2+}\} \cdot \{\text{SO}_4^{2-}\}}{K_{\text{sp}}} \quad (1)$$

where K_{sp} is the solubility product of calcium sulfate (mol^2/L^2), $\{\text{Ca}^{2+}\}$ and $\{\text{SO}_4^{2-}\}$ are the activity of calcium and sulfate, respectively.

$$\text{Re} = \frac{\rho \cdot u \cdot d_h}{\mu} \quad (2)$$

where ρ is the solution density (kg/m^3), μ is the viscosity ($\text{Pa}\cdot\text{s}$), u is the average velocity in the feed channel of the membrane (m/s), and d_h is the hydraulic diameter of the membrane channel (m).

Each experiment was conducted for 120–420 min to enable sufficient coverage of the membrane surface so as to obtain a significant permeate flux decline. Before the first experiment, the membrane was conditioned according to the manufacturer's specifications. At the end of each experiment, the membrane was cleaned using 1% Na_4EDTA at pH 12. All experiments were conducted in duplicates. The reported values are based on the average of the duplicate runs as excellent reproducibility was obtained. An example is given in Fig. 1, which displays two repeat experiments performed at SI of 3.7 and a Re number of 6902.

As shown in Fig. 2, the membrane permeability increased gradually with the number of experiments over time (i.e., the time passed elapsed (days) from the first time a membrane was used). This can be related to the frequency of the chemical cleaning after each experiment, which damages the membrane. For this reason, the membrane permeability, which changes as the membrane deteriorates, is one of three parameters of the developed model (Section 3).

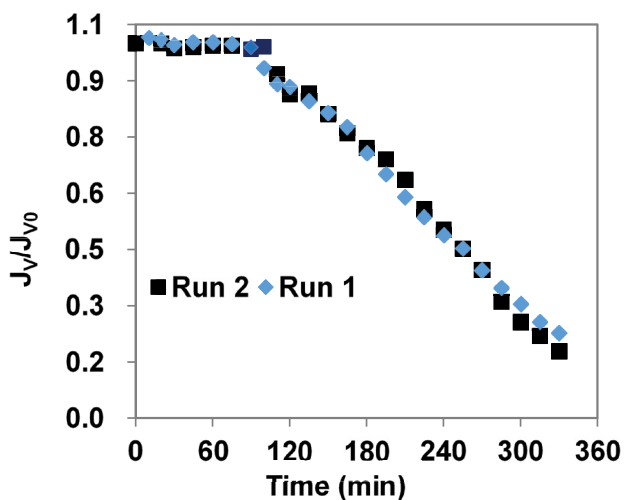


Fig. 1. Repeatability of measurements illustrated by data of two runs (SI = 3.7 and Re = 6902).

3. Model development

The present model aimed to determine the onset of membrane scaling, to ensure efficient operation and maintenance. The scaling onset due to supersaturation assumes a mechanism of crystal growth/deposition on the membrane surface followed by dissolution/removal of the crystals until the rate of scale removal is overruled by the rate of deposition. The net deposition rate reduces the permeability by increasing surface coverage and decreasing the flux with the operation time. The time span between the beginning of operation and the observed onset of flux decline is considered the induction period τ . The model is assigned to provide this time.

Time-dependent concentration distribution develops as a result of the flow conditions, salt convection and diffusion within the flow bulk and its deposition and removal rates from the flow to and of the membrane surface respectively, along the membrane. However, crystal growth and membrane clogging continue to develop when supersaturation occurs adjacent to the membrane surface. This scaling mechanism is like a time dependent mass balance between two simultaneous and opposing transport processes of deposition to and removal from a heat transfer surface in evaporative desalination and other processes [25].

Simulation of the scaling process was conducted using a CFD model (Comsol Multiphysics 5.2a modules) for the annulus membrane system described in Fig. 3. For $\text{Re} < 2000$, a steady-state laminar flow module was used, and for the flow of $\text{Re} \geq 2000$, a turbulent module $k-\epsilon$ was used. Concentration distribution within the flow was simulated by the time-dependent convection and diffusion module, and the scaling stage was simulated by the rate deposition and surface reaction module of CaSO_4 on the active surface of the membrane. The three modules are fully coupled as follows: the CaSO_4 solution flows steadily along the tubular annulus, yielding a velocity profile within the bulk. Because of the CaSO_4 scaling flux from the bulk to the membrane surface, the solute concentration distribution

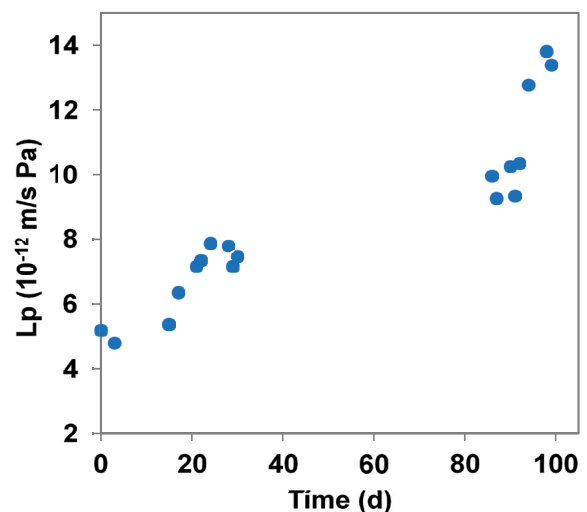


Fig. 2. Membrane permeability change with the time elapsed from its first use.

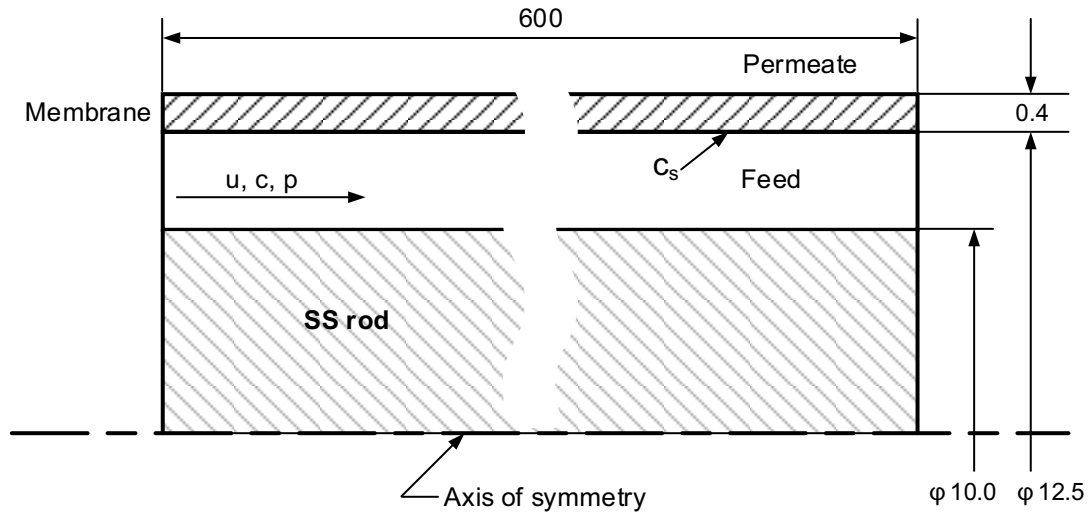


Fig. 3. Schematics of the RO tubular membrane system. A stainless-steel rod was located inside the tubular membrane in order to minimize the flow volume close to the membrane.

changes over time within the flow volume and along the membrane surface.

The required initial and boundary conditions for the flow and convection/diffusion were set. The scaling stage consists of two simultaneous processes: deposition and removal represented by rate coefficients k_a (m³/s mol) and k_r (1/s), respectively, as in Turek et al. [24]. The experimental results revealed that the induction periods varied with the flow conditions and initial membrane permeability. For $t < \tau$ the removal process is the dominant, and it decreases with time, increasing membrane coverage. When $t > \tau$ deposition becomes predominant, resulting in membrane surface coverage and correspondingly, flux decline. The possible function of the removal rate coefficient that accounts for its decay with time was chosen as:

$$k_r = ae^{-k_n t} \quad (3)$$

where a is the removal (detachment) rate constant (1/s) and $e^{-k_n t}$ is the detachment decay term in which k_n is the nucleation rate constant (1/s). The higher k_n the earlier the deposition starts, resulting in shorter induction periods and vice versa. The formulation of k_n accounts for observed variations in the induction period. The overall changes in the flow concentration and in the scaling layer can be given by Eq. (4) which is similar to other kinetic rate equations [26,27].

$$\frac{dC_s}{dt} = k_a C \cdot (C_{s,max} - C_s) - k_r C_s \quad (4)$$

where C is the bulk flow concentration adjacent to the membrane surface (mol/m³), C_s is the surface concentration of the scale (mol/m²), and $C_{s,max}$ is the maximum concentration at the membrane surface (mol/m²) determined by the model fit to the experimental data.

Solution parameters used in the model include dynamic viscosity η (Pa·s) = $8.9 \times 10^{-4} + 5.92 \times 10^{-7} C$ (mol/m³),

diffusivity $D = 8.68 \times 10^{-10}$ (m²/s), solution density ρ (kg/m³) = $997.2 + 0.151 C$ (mol/m³) and osmotic pressure π (Pa) = $1.246 \times 10^4 C$ (mol/m³) + 450. The maximum concentration of calcium sulfate at the membrane surface was found to be $C_{s,max} = 2 \times 10^{-4}$ (mol/m²).

RO permeate flux, J_v , was calculated by:

$$J_v = L_p (\Delta p - \Delta \pi) \quad (5)$$

where L_p is the membrane permeability coefficient (m/s Pa), Δp is the hydraulic pressure differential across the membrane (Pa), and $\Delta \pi$ is the osmotic pressure differential across the membrane (Pa).

Scaling coverage fraction θ of the membrane surface is assumed to be linear with the surface concentration C_s and the flux J_v [9] as:

$$\theta = \frac{C_s}{C_{s,max}}, \quad \frac{J_v}{J_{v,0}} = 1 - \theta \quad (6)$$

where $J_{v,0}$ is the initial permeate flux (m/s) and $1 - \theta$ the uncovered membrane surface.

Boundary conditions of the scaling rate module, used in the CFD model, was set by combining Eqs. (3)–(6). It is in the form of coverage rate of the membrane surface:

$$\frac{d\theta}{dt} = k_a c (1 - \theta) - k_r \theta \quad (7)$$

Eq. (7) links the flow concentration C adjacent to the membrane surface and the membrane surface concentration C_s . It serves as a boundary condition for the CFD model's surface reaction module.

4. Results and discussion

The observed induction period τ_v , for the duplicate experiments listed in Table 1, was determined as the time

Table 1
Experimental conditions, observed and theoretical induction periods, model parameters, and evaluated induction period

Exp. #	SI	Re	L_{p0} (10^{-12} m/s Pa)	τ_o (min)	k_a (10^{-10} m ³ /mol s)	k_n (10^{-3} 1/s)	τ_i (min)	τ_L (min)	σ	EIP (min)
1	4.2	6902	6.6	60	5.0	1.8	63.3	69.2	2.3	49.0
2	2.5	6902	5.6	240	5.9	0.5	260.0	272	14.1	245.7
3	3.2	1233	9.7	25	2.2	2.5	45.0	48.7	14.1	30.7
4	3.2	2938	10.8	50	2.8	1.7	64.5	73.5	10.2	50.2
5	4.2	2938	5.5	20	5.1	3.4	31.9	34.7	8.4	17.6
6	2.1	404	4.9	50	1.0	2.7	55.0	44.8	3.5	40.7
7	3.2	6902	7.2	122	4.6	1.0	121.0	128	0.7	106.7
8	2.1	2938	4.5	160	1.8	0.9	155.7	148	3.0	141.4
9	2.5	404	11.6	25	0.1	3.2	38.0	37.2	9.2	23.7
10	1.8	404	6.8	45	0.2	3.0	42.0	39.9	2.1	27.7
11	3.2	5285	9.3	80	1.9	1.3	100.0	101	14.1	85.7
12	3.7	6902	4.3	95	3.7	1.4	90.0	90.1	3.5	66.7

at which the permeate flux decline was initiated, as indicated by a green circle in Fig. 4a. The observed induction period reflects the upper time limit of scale-free operation beyond which the membrane may be subject to irreversible damage. To minimize clean in place (CIP) frequency, an evaluated induction period is proposed. The EIP should be as close as possible to the observed induction time but lower than it. The EIP is based on the differences between the theoretical and observed induction periods. The latter was determined by the CFD model. Initially, a theoretical permeate flux ($J_v(t)$) was fitted to the experimental flux, yielding adjusted model parameters k_n and k_a (Eqs. (3) and (7), respectively).

The theoretical induction period τ_i was determined by the intersection point of the initial tangent line of the theoretical $J_v(t)$ curve with the tangent line at the inflection point of the mirror S-shaped curve, as displayed in Fig. 4a. The observed induction periods τ_o the model parameters k_a , k_n , and the theoretical induction periods τ_i ,

are summarized in Table 1. The removal rate a (9.5×10^{-4} 1/s (Eq. (3)) was found to be similar for all the experimental data sets. This may suggest that the removal rate mechanism from the membrane in the laminar sub-layer is common to all cases. With known k_a and k_n the CFD model provided theoretical $J_v(t)$ such as the blue curve in Fig. 4a. The theoretical induction periods τ_i were determined and correlated to τ_o (Fig. 4b). The average standard deviation between τ_i and τ_o yielded the EIP listed in Table 1 (Section 4.2).

The model also enables one to determine the fraction of the surface coverage by the scale, θ , along the membrane as a function of the calcium sulfate concentration, as defined in Eq. (6). An example is displayed in Fig. 5. An increase in the surface coverage along the membrane is observed, resulting in the highest surface coverage at the membrane's back end. This coverage profile is in agreement with [1]. The average surface coverage fraction of scaling at the induction periods was found to be 0.066 ± 0.034 .

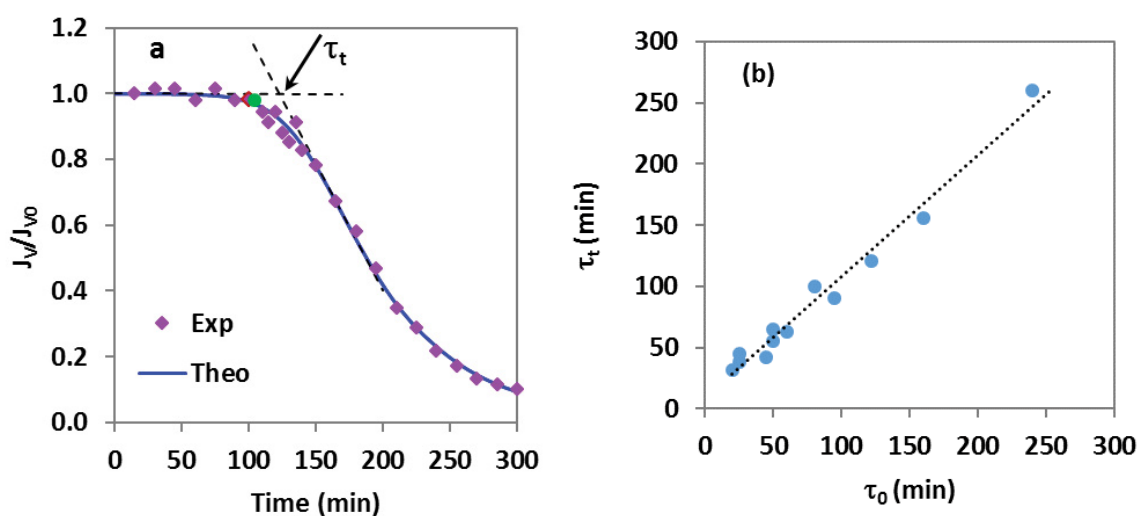


Fig. 4. Observed (experimental) and theoretical (model) (a) normalized flux decline with time due to CaSO_4 scaling (Exp. 7; SI = 3.2; Re = 6902) and (b) induction periods.

4.1. Relationship between the induction period and the rate of deposition

This section provides a theoretical relationship between the induction period and the deposition rate coefficient k_d . The removal rate of CaSO_4 is dominant at the early crystallization stage when $t < \tau_i$. It decays with time according to the assumed Eq. (3). Simultaneously, the deposition or scaling rate increases with time. For $t > \tau_i$ the scaling rate increases sharply due to the vanishing effect of removal as described in Eq. (3). In other words, the induction period terminates when the removal effect practically becomes negligible. Beyond the induction period, scaling becomes the only dominant process, resulting in flux decline. Therefore, deposition accelerates for $t > \tau_i$.

According to the removal assumption in Eq. (3) k_r decreases with time and practically vanishes at $t = \tau_i$. Therefore, the average k_r within the range $0 \leq t \leq \tau_i$ is given by:

$$k_{r,av} \tau_i = \int_0^{\tau_i} k_r dt = \frac{9.5 \cdot 10^{-4} [1/s]}{k_n} (1 - e^{-k_n \tau_i}) \quad (8)$$

Eq. (8) represents the average rate of the removed scale at time $t = \tau_i$. The plot of Eq. (8) vs. τ_i is shown by the dots in Fig. 6. The τ_i in Eq. (8) is replaced by τ_L the induction period along the average line in Fig. 6. The Eq. (9) is derived from the fit line of Eq. (8) with k_n and τ_i values given in Table 1:

$$\frac{9.5 \cdot 10^{-4}}{k_n} (1 - e^{-k_n \tau_L}) = 1.206 \cdot 10^{-4} \cdot \tau_L + 0.034, \quad \tau_L (s), \quad k_n (1/s) \quad (9)$$

A graphic presentation of Eq. (9) in Fig. 7 shows that k_n decreases sharply at short induction periods τ_L . Slower decrease of k_n is observed for longer τ_L . The unique relationship between k_n and τ_L means that the induction period depends only on the deposition rate coefficient. The higher k_n the shorter the τ_L . The value $1000 k_n \tau_L$ displayed in Fig. 7, is \approx constant with an average value of 122.7 ± 4.5 (error of 3.7%). This is in agreement with the theory of the induction time being inversely proportional to the nucleation rate [28].

4.2. Evaluated induction period

From a practical point of view, evaluation of induction periods is needed as a quick and cheap tool to maximize membrane operational time, minimize CIP frequencies, and avoid irreversible membrane damages.

Because the permeate flux measurements and the determination of the observed induction period are both subject to uncertainty, the standard deviation – σ between the observed and theoretical induction periods was calculated. The results are summarized in Table 1. The average standard deviation between the theoretical and observed induction periods was found to be 7.1 min. In order to ensure safety margins (for ~95% of the cases), the EIP was defined as:

$$\text{EIP} = \tau_i - 2\sigma_{\text{Avr}} \quad (10)$$

All the obtained EIP values were below the observed induction time (Table 1). These results satisfy both economic and membrane integrity conditions. It is also evident

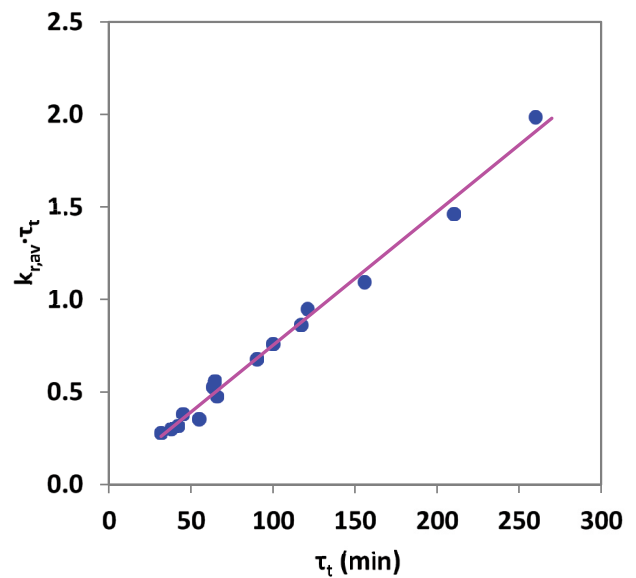


Fig. 6. Presentation of $k_{r,av} \cdot \tau_i$ vs. τ_i (dots), the line is attributed to $k_{r,av} \cdot \tau_L$ vs. τ_i .

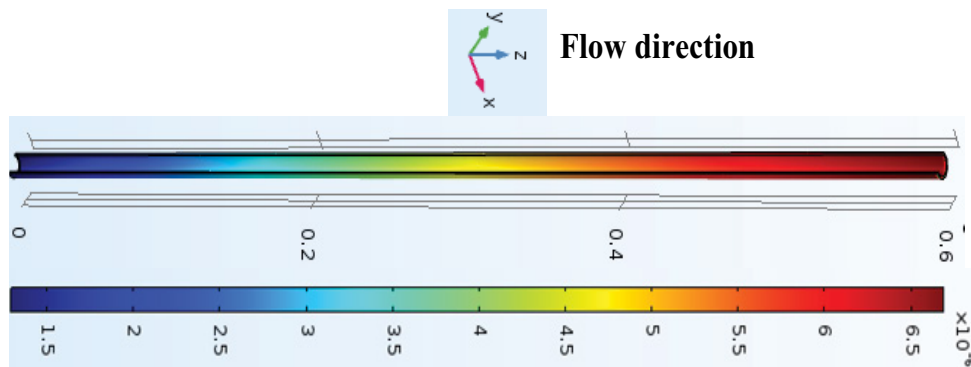


Fig. 5. Surface coverage fraction along the tubular membrane of Exp. 1 (upper line). Lower line is the scale values of colors.

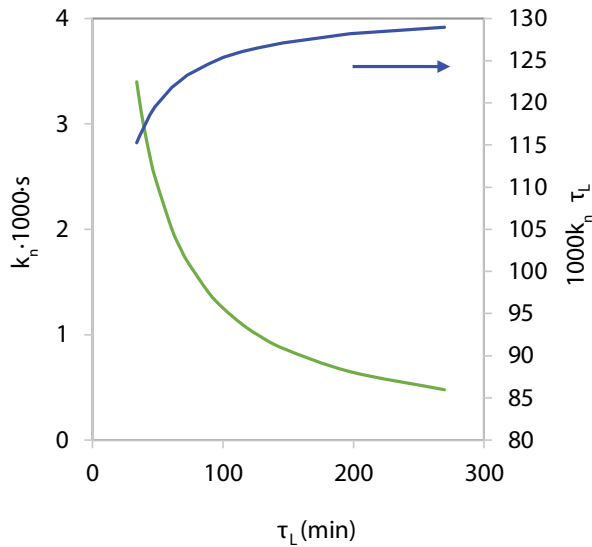


Fig. 7. Graphical presentation of Eq. (9) which relates k_n to τ_L .

(Fig. 8) that the EIP drops with the supersaturation of the solution (Exp. 1, 2, 7 and 12; $Re = 6902$) and increases with the Re number (Exp. 3, 4, 7 and 11; $SI = 3.2$). The results in Fig. 8 show a linear moderate increase in EIP with Re and a sharp decrease with SI . These trends are consistent with Li et al. [2].

To summarize, these are the steps for obtaining the EIP. For a given data set of membrane permeability, $J_v(t)$, SI and Re number, k_n and k_a are adjusted (Eqs. (3) and (7)) by fitting the CFD model to the experimental data of flux vs. time. Next, the theoretical τ_t is calculated as described in Fig. 4a for each data set. The average standard deviation between the observed and theoretical induction periods was calculated. Finally, EIP was determined by subtracting the value of two average standard deviations for the theoretical induction period (Eq. (10)).

5. Concluding remarks

An evaluation tool, in the form of a CFD model, for the induction period of calcium sulfate scaling on RO membranes was introduced. The model fully couples the solution flow, convection, and diffusion of the $CaSO_4$ in the bulk solution and the deposition/desorption reactions occurring on the membrane surface, resulting in scaling. The observed induction periods were determined by monitoring the permeate flux over time. The onset of scaling was defined as the time when the flux began to decline. The model fitted well to the experimental data, yielding two adjusted parameters: the deposition and removal rate coefficients. Once determined, a theoretical induction period was calculated. Finally, the evaluated induction periods were determined, taking into account the average standard deviation between the observed and theoretical induction periods. These evaluated induction periods were shorter than the observed induction periods, satisfying both economic and membrane integrity conditions. The proposed evaluation tool was introduced

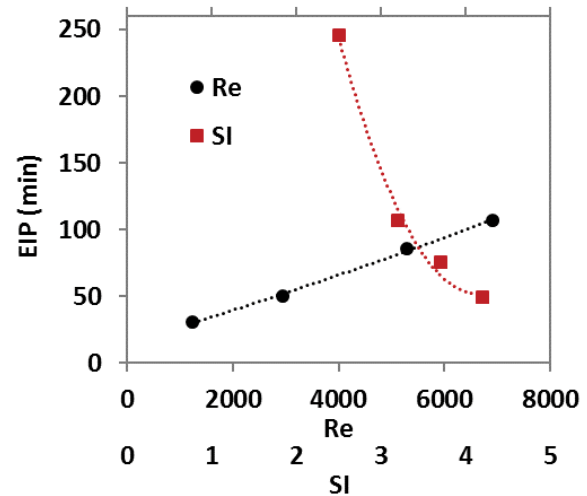


Fig. 8. EIP dependence on flow conditions (Re number) and concentration (SI).

for scaling without the addition of a scale-inhibitor. Yet, there is no doubt that the same approach can be applied to systems operating with scale-inhibitors.

Symbols

a	–	Removal (detachment) rate, 1/s
C	–	Concentration adjacent to the membrane surface, mol/m ³
CFD	–	Computational fluid dynamics
CIP	–	Clean in place
C_s	–	Surface concentration of the scale, mol/m ²
$C_{s,max}$	–	Maximum concentration at the membrane surface, mol/m ²
d_h	–	Hydraulic diameter of the membrane channel, m
D	–	Diffusivity, m ² /s
EIP	–	Evaluated induction periods, min
J_v	–	Permeate flux, m/s
$J_{v,0}$	–	Initial permeate flux, m/s
$J_v(t)$	–	Permeate flux at time t , m/s
k_a	–	Deposition rate coefficient, m ³ /s mol
k_r	–	Removal rate coefficient, 1/s
k_n	–	Nucleation rate constant, 1/s
L_p	–	Membrane permeability coefficient, m/s Pa
K_{sp}	–	Solubility product of calcium sulfate, mol ² /L ²
P	–	Pressure, Pa
Re	–	Reynolds number
SI	–	Saturation index
t	–	Time, s
u	–	Average velocity in the feed channel of the membrane, m/s

Greek letters

η	–	Dynamic viscosity of the solution, Pa s
θ	–	Fractional surface coverage by the scale
μ	–	Viscosity, Pa s
π	–	Osmotic pressure, Pa

ρ	—	Solution density, kg/m ³
σ	—	Standard deviation
σ_{Avr}	—	Average Standard deviation
τ	—	Induction period, min
τ_L	—	Averaged theoretical induction period (min) described in Eq. (9)
τ_o	—	Observed induction period, min
τ_t	—	Theoretical induction period, min

References

- [1] W. Wei, X. Zou, X. Ji, R. Zhou, K. Zhao, Y. Wang, Analysis of concentration polarization in full-size spiral wound reverse osmosis membranes using computational fluid dynamics, *Membranes*, 11 (2021) 353, doi: 10.3390/membranes11050353.
- [2] X. Li, D. Hasson, H. Shemer, Flow conditions affecting the induction period of CaSO₄ scaling on RO membranes, *Desalination*, 431 (2018) 119–125.
- [3] S. Shirazi, C.-J. Lin, D. Chen, Inorganic fouling of pressure-driven membrane processes – a critical review, *Desalination*, 250 (2010) 236–248.
- [4] A. Antony, J.H. Low, S. Gray, A.E. Childress, P. Le-Clech, G. Leslie, Scale formation and control in high pressure membrane water treatment systems: a review, *J. Membr. Sci.*, 383 (2011) 1–16.
- [5] C.Y. Tang, T.H. Chong, A.G. Fane, Colloidal interactions and fouling of NF and RO membranes: a review, *Adv. Colloid Interface Sci.*, 164 (2011) 126–143.
- [6] T.A. Hoang, Chapter 3 – Mechanisms of Scale Formation and Inhibition, Z. Amjad, K.D. Demadis, Eds., *Mineral Scales and Deposits: Scientific and Technological Approaches*, 1st ed., Elsevier, eBook ISBN: 9780444627520, 2015, pp. 47–83.
- [7] P.S. Goh, W.J. Lau, M.H.D. Othman, A.F. Ismail, Membrane fouling in desalination and its mitigation strategies, *Desalination*, 425 (2018) 130–155.
- [8] A. Ruiz-García, N. Melián-Martel, I. Nuez, Short review on predicting fouling in RO desalination, *Membranes*, 7 (2017) 62–79.
- [9] J. Gilron, D. Hasson, Calcium sulfate fouling of reverse osmosis membranes: flux decline mechanism, *Chem. Eng. Sci.*, 42 (1987) 2351–2360.
- [10] J. Borden, J. Gilron, D. Hasson, Analysis of RO flux decline due to membrane surface blockage, *Desalination*, 66 (1987) 257–269.
- [11] M. Brusilovsky, J. Borden, D. Hasson, Flux decline due to gypsum precipitation on RO membranes, *Desalination*, 86 (1992) 187–222.
- [12] E. Fountoukidis, Z.B. Marouls, D. Marinos-Kouris, Modeling of calcium sulfate fouling of reverse osmosis membranes, *Desalination*, 72 (1989) 294–318.
- [13] J. Li, L.J. Koen, D.K. Hallbauer, L. Lorenzen, R.D. Sanderson, Interpretation of calcium sulfate deposition on reverse osmosis membranes using ultrasonic measurements and a simplified model, *Desalination*, 186 (2005) 227–241.
- [14] D.P. Logan, S. Kimura, Control of gypsum scale on reverse osmosis membranes, *Desalination*, 54 (1985) 321–331.
- [15] H.J. Oh, Y.K. Choung, S. Lee, J.S. Choi, T.M. Hwang, J.H. Kim, Scale formation in reverse osmosis desalination: model development, *Desalination*, 238 (2009) 333–346.
- [16] E. Lyster, J. Au, R. Rallo, F. Giral, Y. Cohen, Coupled 3-D hydrodynamics and mass transfer analysis of mineral scaling-induced flux decline in a laboratory plate-and-frame reverse osmosis membrane module, *J. Membr. Sci.*, 339 (2009) 39–49.
- [17] A.I. Radu, L. Bergwerff, M.C.M. van Loosdrecht, C.A. Picoreanu, A two-dimensional mechanistic model for scaling in spiral wound membrane systems, *Chem. Eng. J.*, 241 (2014) 77–91.
- [18] I. Janghorban Esfahani, M.J. Kim, C.H. Yun, C.K. Yoo, Proposed new fouling monitoring indices for seawater reverse osmosis to determine the membrane cleaning interval, *J. Membr. Sci.*, 442 (2013) 83–96.
- [19] O. Söhnel, J. Garside, *Precipitation: Basic Principles and Industrial Applications*, Butterworth-Heinemann, Oxford, 1992.
- [20] M.C. Van der Leeden, D. Verdoes, D. Kashchiev, G.M. van Rosmalen, Induction Time in Seeded and Unseeded Precipitation, J. Garside, R.J. Davey, A.G. Jones, Eds., *Advances in Industrial Crystallization*, Butterworth-Heinemann, Oxford, 1991, pp. 31–46.
- [21] N. Epstein, *Particulate Fouling of Heat Transfer Surfaces: Mechanisms and Models*, L.F. Melo, T.R. Bott, C.A. Bernardo, Eds., *Fouling Science and Technology*, NATO ASI Series (Series E: Applied Sciences), Vol. 145, Springer, Dordrecht. https://doi.org/10.1007/978-94-009-2813-8_10, 1988, pp. 143–164.
- [22] S. Mitrouli, A.J. Karabelas, A. Karanasiou, M. Kostoglou, Incipient calcium carbonate scaling of desalination membranes in narrow channels with spacers-experimental insights, *J. Membr. Sci.*, 425–426 (2013) 48–57.
- [23] A.J. Karabelas, A. Karanasiou, S.T. Mitrouli, Incipient membrane scaling by calcium sulfate during desalination in narrow spacer-filled channels, *Desalination*, 345 (2014) 146–157.
- [24] M. Turek, K. Piotrowski, P. Dydo, K. Mitko, E. Bernackac, A. Jakóbk-Kolon, Mathematical modeling of scaling-free membrane module by combining residence time distribution, metastability, and induction time, *Desal. Water Treat.*, 214 (2021) 312–320.
- [25] D.Q. Kern, R.E. Seaton, Surface fouling – How to calculate limits, *Chem. Eng. Prog.*, 55 (1959) 71–73.
- [26] R. Karlsson, A. Michaelsson, L. Mattsson, Kinetic analysis of monoclonal antibody-antigen interactions with a new biosensor based analytical system, *J. Immunol. Methods*, 145 (1991) 229–240.
- [27] S.M. Aghaei, M.M. Monshi, I. Calizo, A theoretical study of gas adsorption on silicone nanoribbons and its application in a highly sensitive molecule sensor, *RSC Adv.*, 6 (2016) 94417–94428.
- [28] D. Hasson, A. Dark, R. Semiat, Induction times induced in an RO system by anti-scalants delaying CaSO₄ precipitation, *Desalination*, 157 (2003) 193–207.